UCLA-ENG-7638
APRIL 1976

INTERACTIONS OF SATELLITE-SPEED HELIUM ATOMS WITH SATELLITE SURFACES
II: ENERGY DISTRIBUTIONS OF REFLECTED HELIUM ATOMS

S.M. LIU
E.L. KNUTH

UCLA • SCHOOL OF ENGINEERING AND APPLIED SCIENCE

UCLA-ENG-7638
APRIL 1976

INTERACTIONS OF SATELLITE-SPEED HELIUM ATOMS WITH SATELLITE SURFACES

II: ENERGY DISTRIBUTIONS OF REFLECTED HELIUM ATOMS

by

S. M. Liu

E. L. Knuth

School of Engineering and Applied Science
University of California
Los Angeles, California

FOREWORD

The researches described here were supported mainly by the National Aeronautics and Space Administration (under Grant NGR 05-007-416) and by the UCLA School of Engineering and Applied Science. These studies were part of a continuing program of researches in gas-surface interactions.

ABSTRACT

Energy transfer in collisions of satellite-speed (7000 m/sec) helium atoms with a cleaned 6061-T6 satellite-type aluminum surface was investigated using the molecular-beam technique. The amount of energy transferred was determined from the measured energy of the molecular-beam and the measured spatial and energy distributions of the reflected atoms.

Spatial distributions of helium atoms scattered from a 6061-T6 aluminum surface were measured again in this study, and show features similar to those presented in report UCLA-ENG-7546 [1]. The scattering pattern exhibits a prominent backscattering, probably due to the gross surface rougnesss and/or the relative lattice softness of the aluminum surface.

Energy distributions of reflected helium atoms from the same surface were measured for six different incidence angles. For each incidence angle, distributions were measured at approximately sixty scattering positions. At a given scattering position, the energy spectra of the reflected helium atoms and the background gas were obtained using the retarding-field energy analyzer. The mean reflected-beam energy and the differential energy accommodation coefficient ($(A.C.)_E(\theta_i,\theta_r,\phi)$) were then extracted from these spectra using a least-square fitting program. The measured $(A.C.)_E(\theta_i,\theta_r,\phi)$s show some fluctuations and a weak dependence on scattering angle, i.e., the accommodation decreases slowly as the scattering direction shifts toward the surface tangent.

The overall energy accommodation coefficient for a beam with a given incidence angle was then evaluated using the measured spatial density distributions and the mean reflected-beam energy distributions. Results show that the mean accommodation coefficient varies between 50% and 65%, dependent on the incidence angle.

TABLE OF CONTENTS

LIST OF FIGURES

LIST OF TABLES

LIST OF SYMBOLS

$(A.C.)_E(\theta_i,\theta_r,\phi)$	differential energy accommodation coefficient at scattering position (θ_r,ϕ) for a beam with θ_i incidence angle
$\overline{(A.C.)_E(\theta_i)}$	overall energy accommodation coefficient for a beam with θ_i incidence angle
E_i	incident-beam energy
$E_r(\theta_i,\theta_r,\phi)$	energy of scattered helium atoms at scattering position (θ_r,ϕ) for a beam with θ_i incidence angle
$\tilde{E}_r$	energy of scattered helium atoms evaluated from its differential energy spectrum
$\tilde{E}_{ref}$	mean reference energy of thermal background gas evaluated from its differential energy spectrum
$f(E)$	differential energy distribution
$n_i(\theta_i,\theta_r,\phi)$	normalized spatial density-distribution function
$\hat{n}$	surface normal
$\hat{t}$	surface tangent
θ_i	incidence angle of helium beam measured from surface normal
θ_r	in-plane scattering angle measured from surface normal
ϕ	out-of-plane scattering angle measured from the plane of incidence
σ	standard deviation of the true reflected-beam energy spectrum from the least-square fitted function

CHAPTER I

INTRODUCTION

Basic knowledge concerning energy and momentum transfer between earth satellites and upper-atmospheric gases is essential for understanding the drag experienced by earth satellites (therefore for estimating the lifetime of an earth satellite and/or extracting the mean upper-atmosphere density from satellite drag data). For example, in predicting the aerodynamic drag of a satellite, one uses frequently a model in which the thermal accommodation between the ambient gas and the satellite surface is complete and the scattering distribution of reflected molecules follows the cosine law. However, possible deviations from this model might yield greatly different results.

These energy and momentum transfers can be investigated experimentally in the laboratory using an ultra-high vacuum system and the molecular-beam technique. The desired information can be extracted from the change in the beam properties during the surface collision if the states of both the incident and the scattered beam (spatial distribution and speed distribution) can be determined. Spatial distributions of satellite-speed helium beams scattered from satellite surfaces were obtained previously and summarized in report UCLA-ENG-7546. This report presents measured energy distributions of helium atoms reflected from 6061-T6 aluminum surfaces.

In Chapter II, the experimental apparatus and procedures are described briefly. Emphasis is given on the design and the operating procedure for the retarding-field energy analyzer. Experimental results are given and discussed in Chapter III. A least-square curve-fitting computer program is given in an Appendix.

CHAPTER II

EXPERIMENTAL APPARATUS AND PROCEDURES

The present experimental study was carried out in the UCLA Molecular-Beam Laboratory using the molecular-beam system shown schematically in Figure II-1. Since it has been described in detail elsewhere [1,2], only a brief description will be given here.

The satellite-speed (7000 m/sec) helium beams were generated using an arc-heated supersonic beam source developed by Young [3]. The incident beam was collimated by an orifice of 0.10-inch diameter placed between the collimation chamber and the detection chamber. The beam was characterized by a multi-disk velocity selector located in the collimation chamber.

A new detection system was constructed during the course of this study for facilitating measurements of the complete three-dimensional density and mean-energy distributions of satellite-speed helium atoms reflected from satellite surfaces. Cf. Figure II-2. This new system includes (1) a target positioning mechanism, (2) a detector rotating mechanism and (3) a mass spectrometer and/or a retarding-field energy analyzer. Descriptions of the first two mechanisms were given in the first report of this study (cf. ref. 1). The design and the operating procedure for the retarding-field energy analyzer will be given here.

The retarding-field energy analyzer is shown in Figures II-3 and II-4. An electron-impact ionizer, mounted 0.5-inch from the target surface on the entrance plate of the analyzer, was used to ionize a fraction of the beam species (also of the residual background). The retarding-field section of the analyzer is made of seven thin stainless-steel washer-shaped discs placed in a stainless-steel can. The inlet plate is followed by three

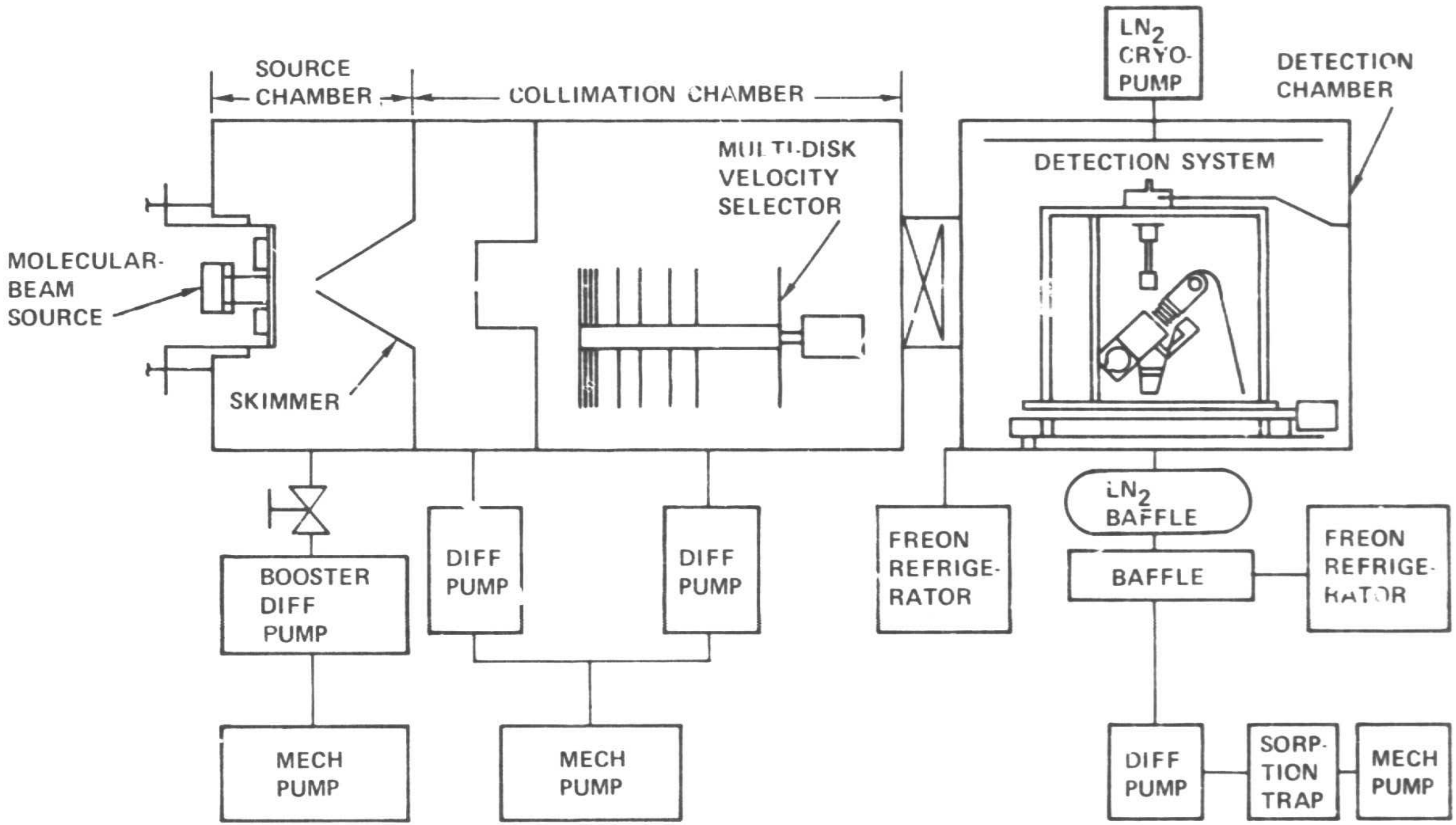

Figure II-1. Schemat.. Diagram of the Molecular Beam System.

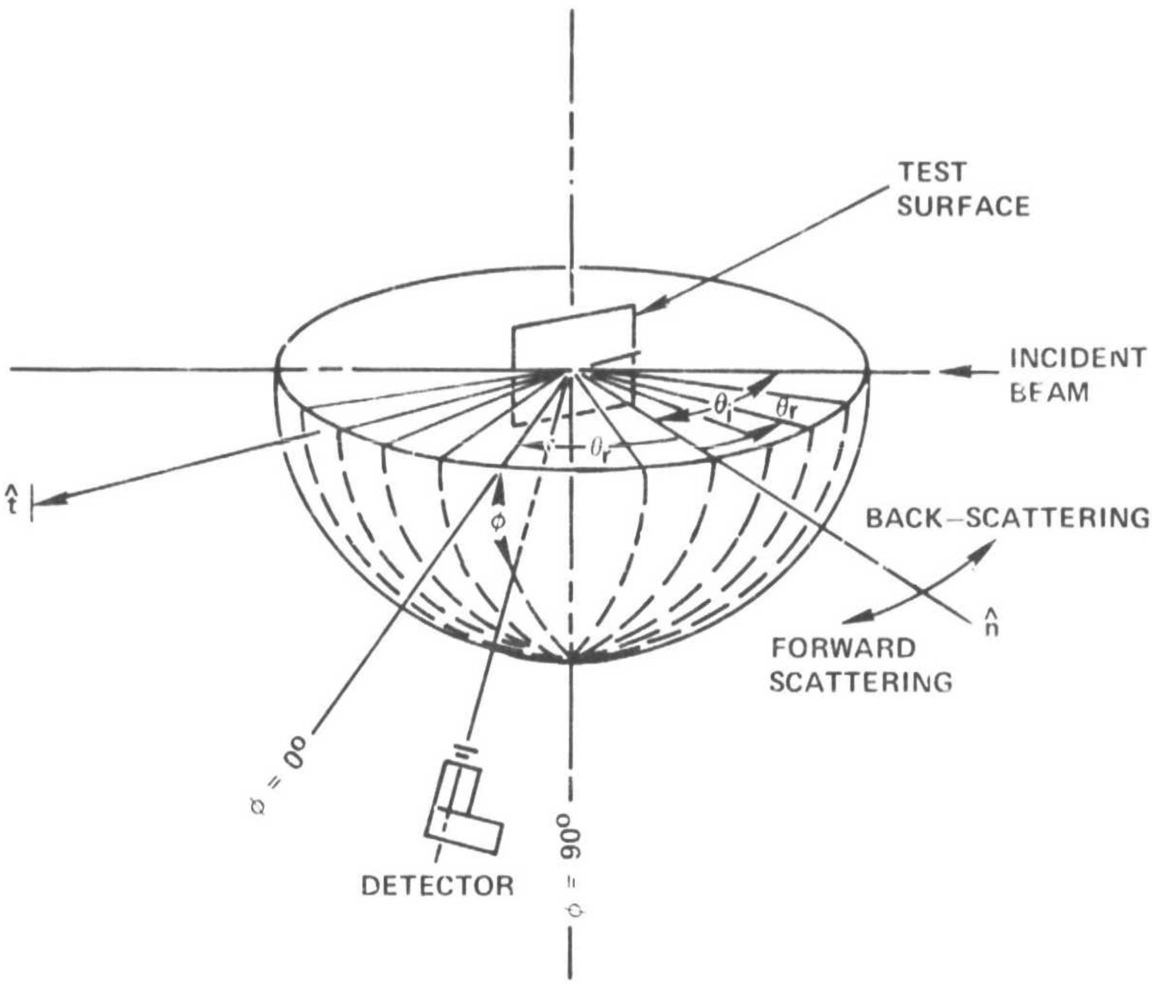

Figure II-2. Schematic Diagram of the Scatter' ıg System.

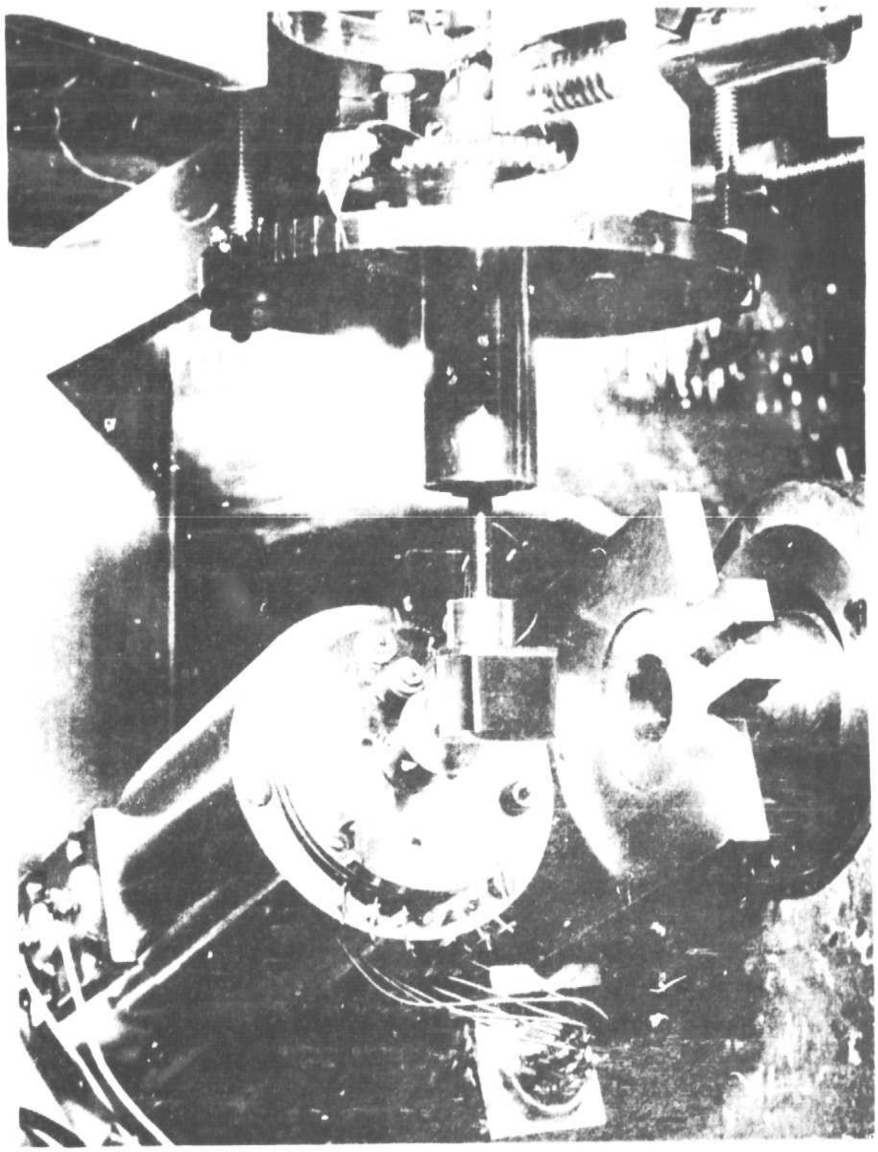

Figure II-3 Photograph of the Retarding Field Energy Analyzer.

PLATE	APERTURE DIA (IN.)	POTENTIAL (V)
1	0.10	GROUND
2	0.25	$V_R - 175$
3	0.25	V_R
4	0.25 (MESH)	$V_R - 175$
5	0.25 (MESH)	V_R
6	0.25 (MESH)	$V_R - 175$
7	0.25	$V_R - 60$

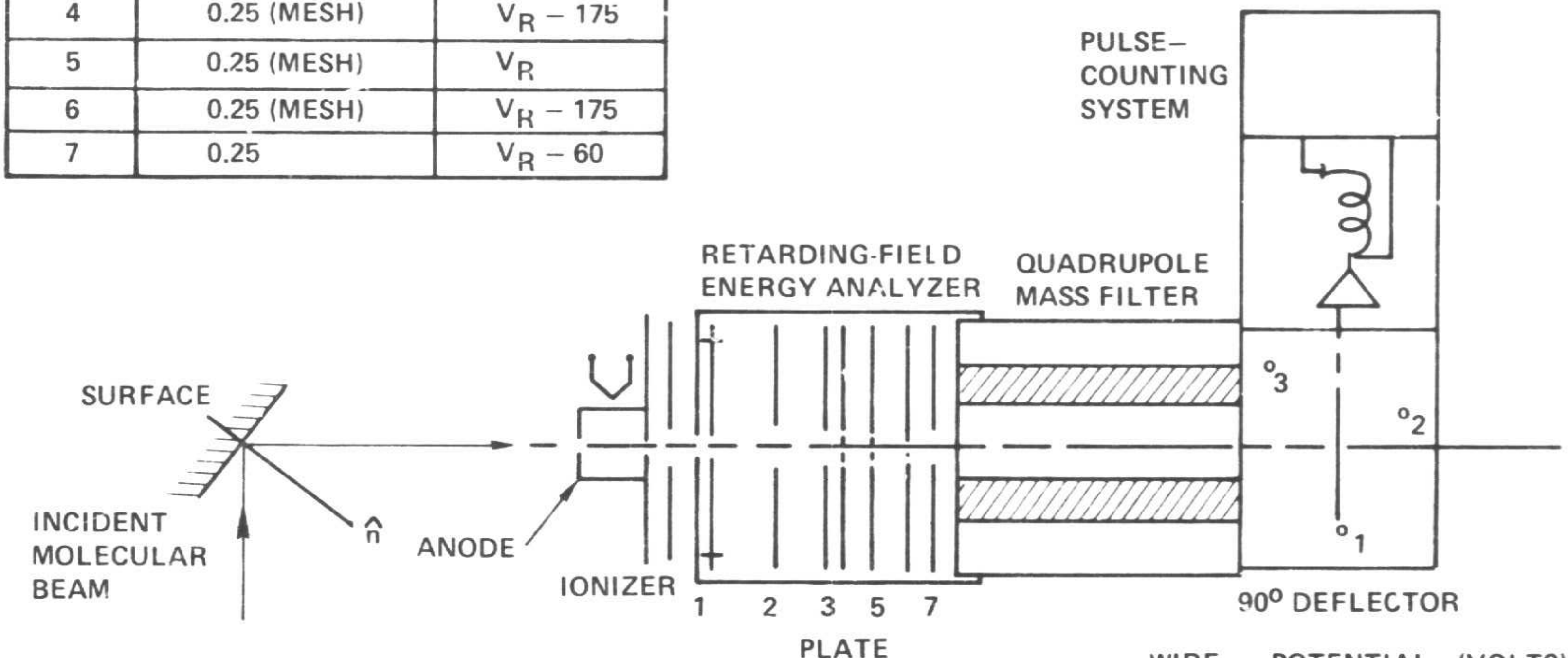

WIRE	POTENTIAL (VOLTS)
1	+50
2	+50
3	-500

Figure II-4. Schematic Diagram of the Retarding-Field Energy Analyzer.

focusing plates, a retarding plate and two more focusing plates. The potentials of all plates except that of the inlet plate are floated relative to the retarding potential so that ions of different energies will experience the same focusing effects within the analyzer. Thus undesirable effects of the energy-dependence of the transmission efficiency are minimized. Typical plate potentials also are given in Figure II-4.

The ions that have passed through the retarding-field region were filtered by a 2-inch quadrupole mass filter to eliminate the noise from the ionized background gases. The filtered ions were then detected by a pulse-counting particle detector. The energy spectrum of the reflected atoms at a given scattering position was obtained by measuring the reflected-beam density as a function of the retarding potential. The measured spectrum was processed by a NS513 signal averager and recorded on IBM cards. A block diagram of the electronic system is shown in Figure II-5.

Although the electron-impact ionization does not change the kinetic energy of a helium atom (since the translational energy transfer between the ionizing electron and the atom is negligible due to the large ratio of their masses), it was found that space-charge effects of ionizing electrons in the ionization region and/or surface-charge effects on the anode cage did introduce a systematic shift of the entire energy spectrum toward lower energies (i.e., the positive ions were produced in a region of negative potential with respect to ground). To reduce this shift, a small emission current ($\sim$ 50 μA) was used in the ionizer. Also, a positive potential (8 volts relative to ground) was applied to the anode cage in order to counter shift the energy spectrum toward higher energies. Then, since the potential of the ionization region was no longer at ground level, it was necessary to

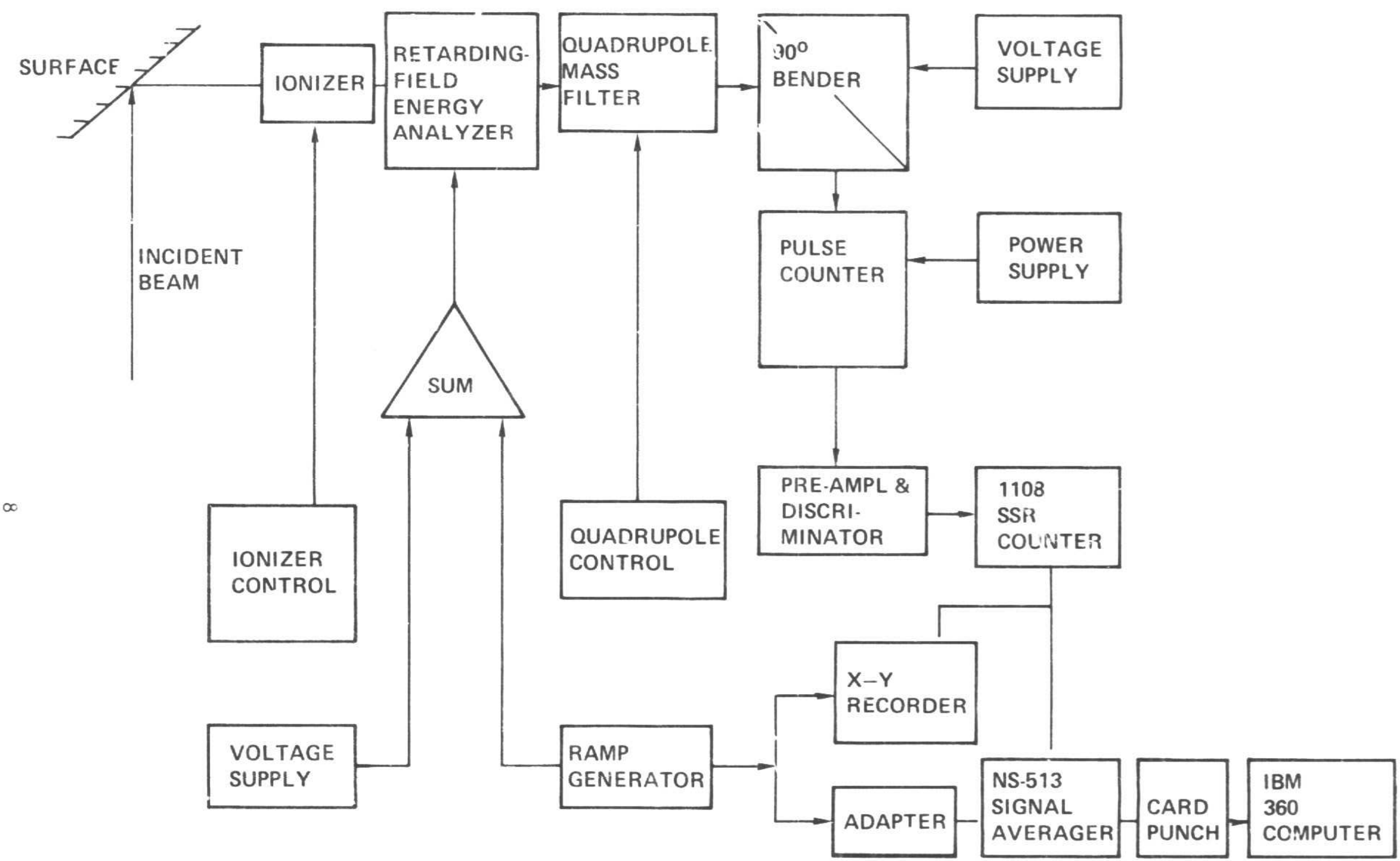

Figure II-5. Block Diagram of the Electronic System of the Retarding-Field Energy Analyzer.

ascertain independently a reference point in the energy spectrum. This reference point was provided by the thermal energy spectrum of the background gas, which has a mean thermal energy of 0.05 eV (i.e., the mean thermal energy at 296°K).

Since the background gas of the beam species also contributed to the measured spectrum, it was necessary to subtract this contribution in order to obtain the reflected-beam energy distributions. This subtraction was facilitated by measuring two spectra (one for the reflected beam plus background and one for the background alone) under the same operating conditions. Both spectra were then processed using a computer program; the reflected-beam energy spectrum was obtained by subtracting the background spectrum from the overall beam-energy spectrum. Both the background spectrum and the reflected-beam spectrum were least-square fitted using a high-order Chebyshev polynomial function. The differential energy distributions f(E) were obtained by simple differentiation of the fitted functions. The mean reflected-beam energy at a given scattering position was evaluated from

$$E_r(\theta_i,\theta_r,\phi) = \tilde{E}_r - \tilde{E}_{ref} + 0.05 \text{ (eV)} \qquad \text{(II-1)}$$

where

$$\tilde{E}(\theta_i,\theta_r,\phi) = \int f(E)\cdot E\cdot dE \Big/ \int f(E)\cdot dE \qquad \text{(II-2)}$$

and 0.05 eV is the thermal energy of the background gas at 296°K. The differential energy accommodation coefficient at a given scattering position was obtained using

$$[A.C.]_E(\theta_i,\theta_r,\phi) = \frac{E_i - E_r(\theta_i,\theta_r,\phi)}{E_i} \qquad \text{(II-3)}$$

where E_i is the incident-beam energy. The computer program and its input parameters for handling the described data reduction are given in the Appendix. The overall energy accommodation for a given incidence angle was then evaluated by

$$\overline{[A.C.]_E(\theta_i)} = \sum_{\theta_r} \sum_{\phi} n_i(\theta_i, \theta_r, \phi) \cdot [A.C.]_E(\theta_i, \theta_r, \phi) \qquad \text{(II-4)}$$

where $n_i(\theta_i, \theta_r, \phi)$ is the normalized spatial density-distribution function of reflected helium atoms.

As indicated, spatial distributions of satellite-speed helium beams scattered from four different satellite surfaces were obtained in the first phase of this study. Experimental procedures and results are included in report UCLA-ENG-7446 [1]. However, spatial distributions at some angles in the backscattering region were not measured at that time due to the constraint on the detector path as indicated in Figure II-6-(a). This problem was solved later by rotating the surface counterclockwise beyond the normal incidence angle while retaining the previous detector path as shown in Figure II-6-(b). Spatial and energy distributions were measured in the present study using these complementary configurations.

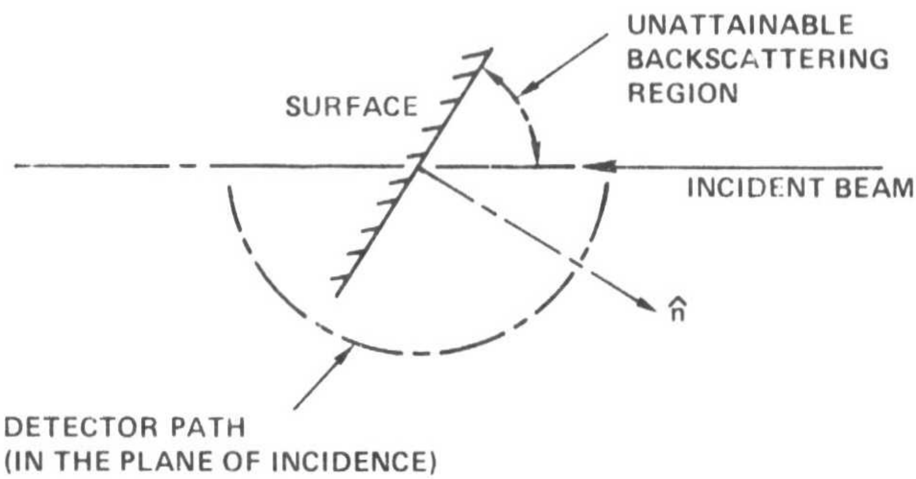

CONFIGURATION (a)

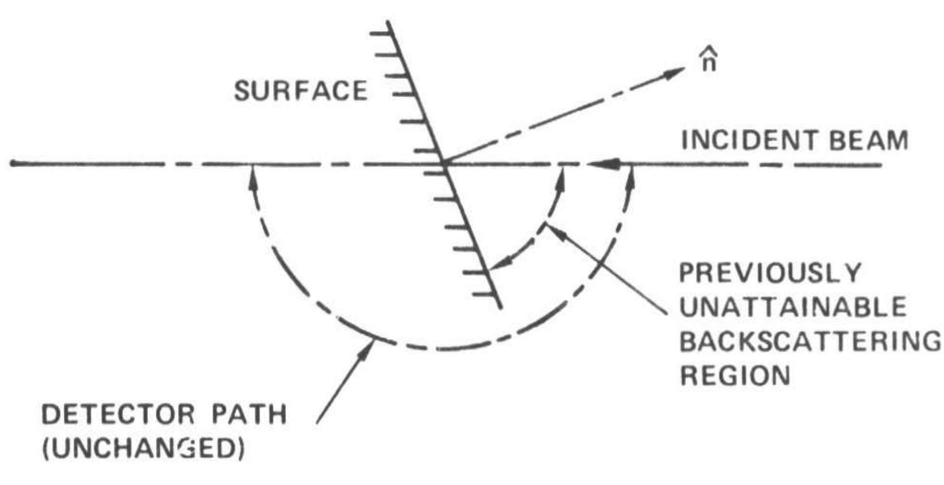

CONFIGURATION (b)

Figure II-6. Complementary Beam-Surface Configurations of the Scattering System.

CHAPTER III

RESULTS AND DISCUSSIONS

Spatial distributions of a satellite-speed (7000 m/sec) helium beam scattered from a cleaned 6061-T6 aluminum satellite surface for six different incidence angles (0°, 15°, 30°, 45°, 60° and 75° from the surface normal) are shown in Figures III-1 to III-6. The center of the polar diagram corresponds to the point of impingement. The incident beam impinges on the test surface (which coincides with the surface of the page) from the bottom of the diagram with the given incidence angle measured from the surface normal. The upper ($\theta_r > 0$) and lower ($\theta_r < 0$) halves of the diagram represent the forward-scattering and backward-scattering regions respectively. The dashed lines at constant value of θ_r indicate detector paths (i.e., from $\phi = 0°$ to $\phi = 90°$). ϕ denotes the out-of-plane scattering angle and $\phi = 0°$ represents the plane of incidence. These results show diffusive scattering patterns and exhibit trends similar to those previously reported [1]. As indicated before, the most interesting feature on these scattering patterns is the prominent backscattering of the incident helium atoms (i.e., a large fraction of the incident atoms are scattered back in the vicinity of the incident beam), particularly as the incidence angle increases toward the surface tangent (i.e., for large values of θ_i). This large fraction of backscattering could be due to the gross surface roughness and/or the relative lattice softness of the aluminum satellite surfaces. Smith [4] observed a large increase in backscattering intensity for increasing surface roughness in his computer simulation of gas molecule reflections from rough surfaces. This backscattering could result in relatively high drag coefficients for such satellite surfaces. The spatial-distribution

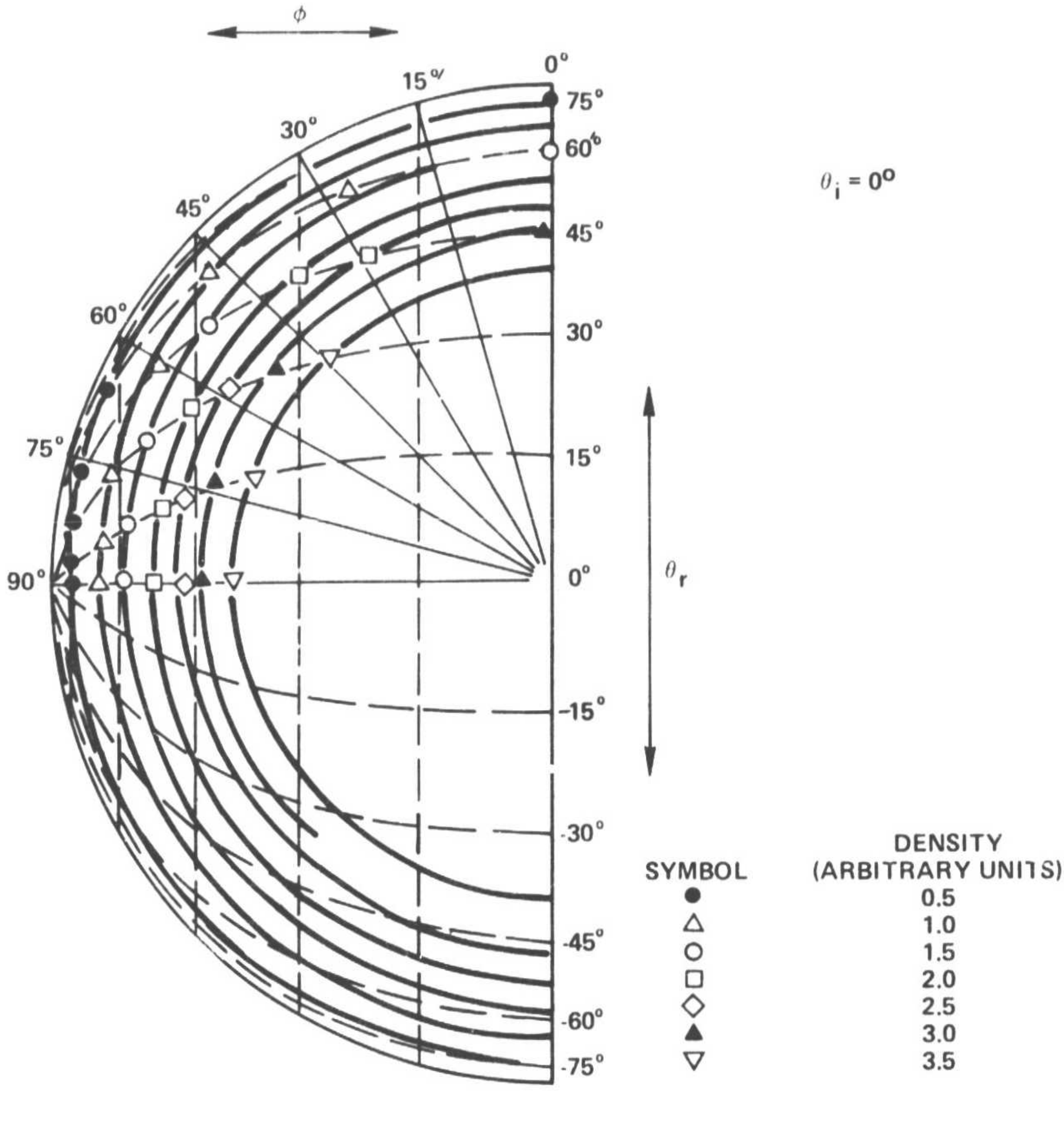

Figure III-1. Polar Plot of Scattered-Beam Density Distribution for 7000 m/sec Helium Beam Scattered from Cleaned 6061-T6 Aluminum Plate at 0° Incidence Angle.

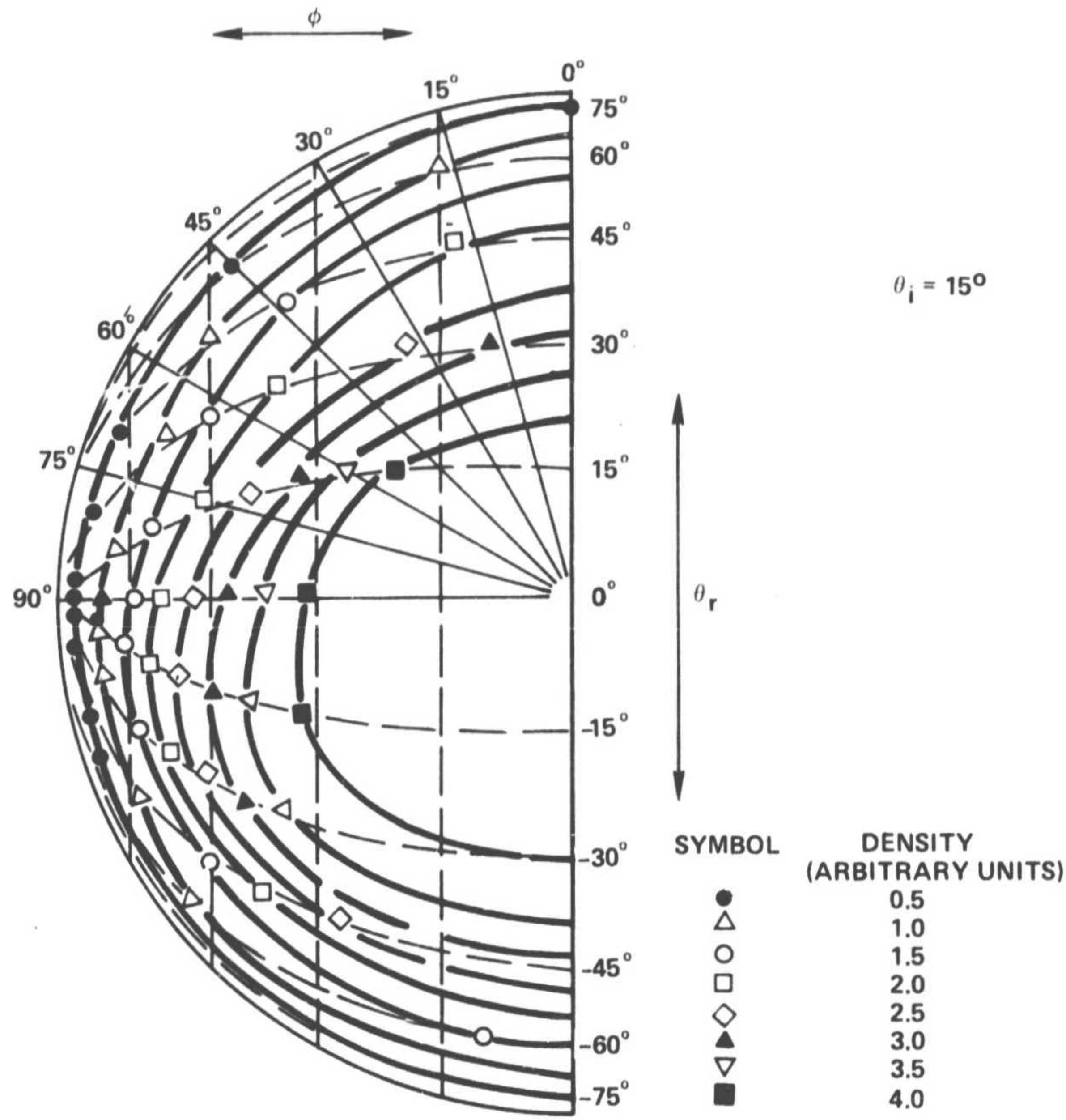

Figure III-2. Polar Plot of Scattered-Beam Density Distribution for 7000 m/sec Helium Beam Scattered from Cleaned 6061-T6 Aluminum Plate at 15° Incidence Angle.

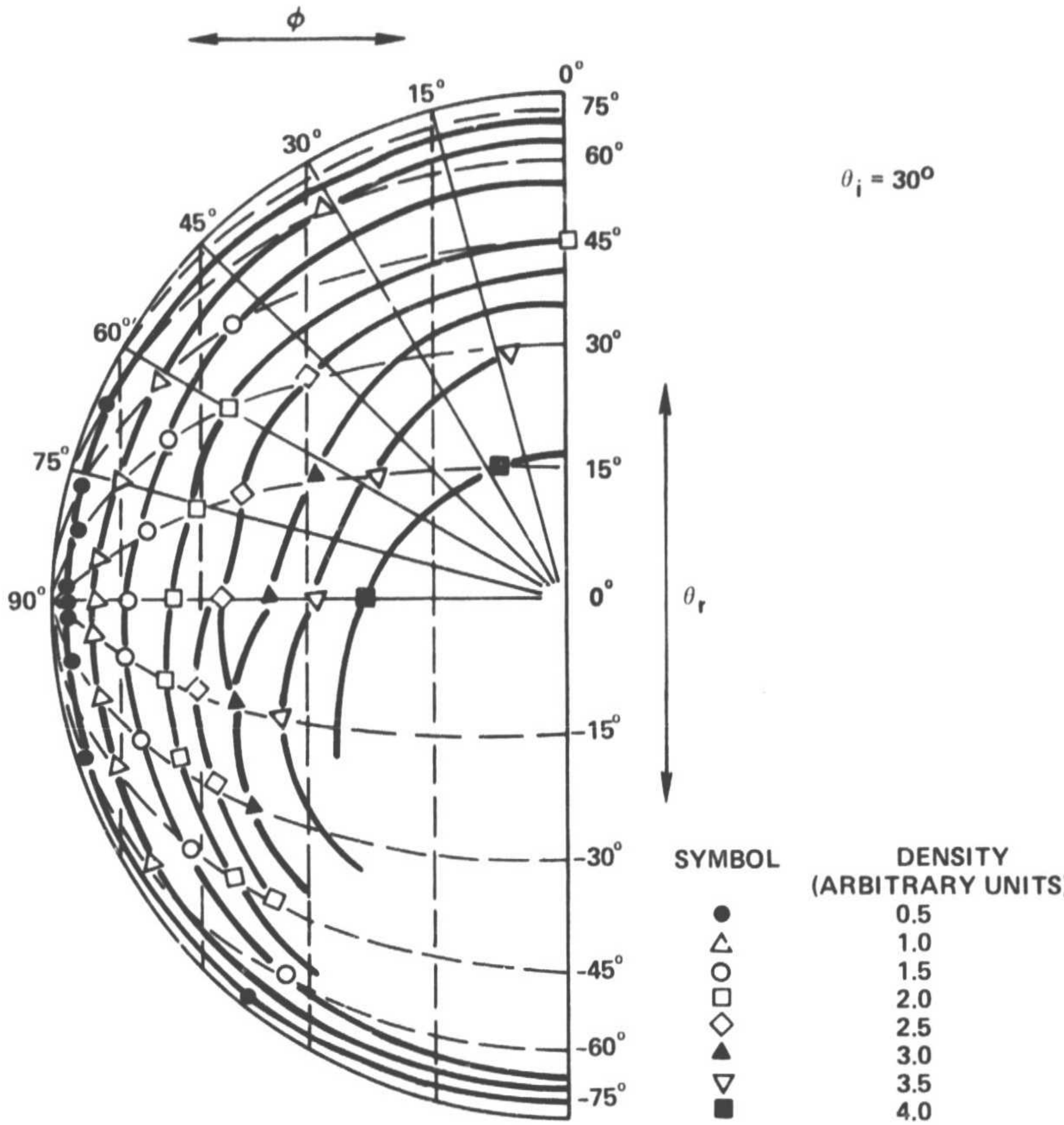

Figure III-3. Polar Plot of Scattered-Beam Density Distribution for 7000 m/sec Helium Beam Scattered from Cleaned 6061-T6 Aluminum Plate at 30° Incidence Angle.

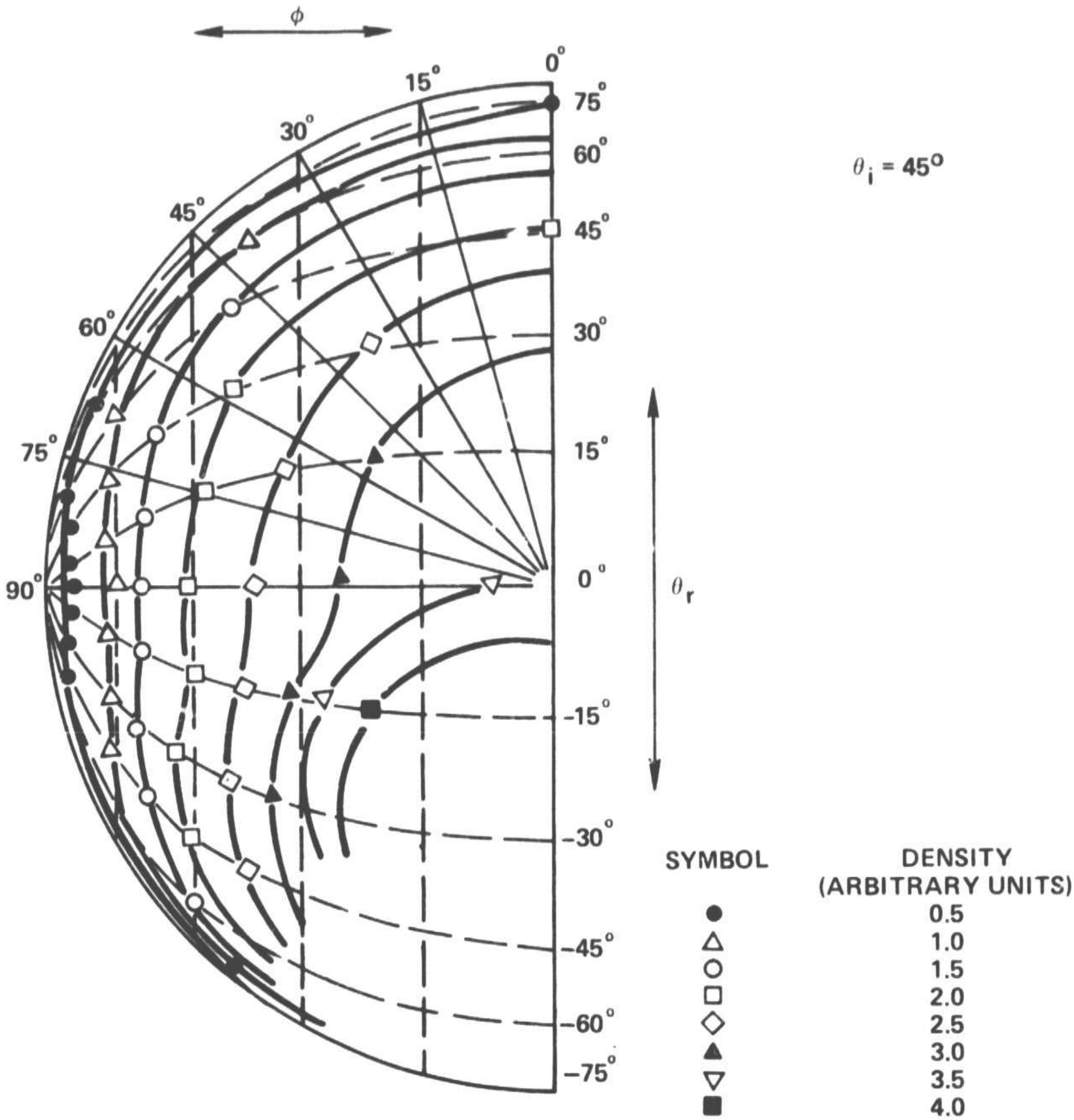

Figure III-4. Polar Plot of Scattered-Beam Density Distribution for 7000 m/sec Helium Beam Scattered from Cleaned 6061-T6 Aluminum Plate at 45° Incidence Angle.

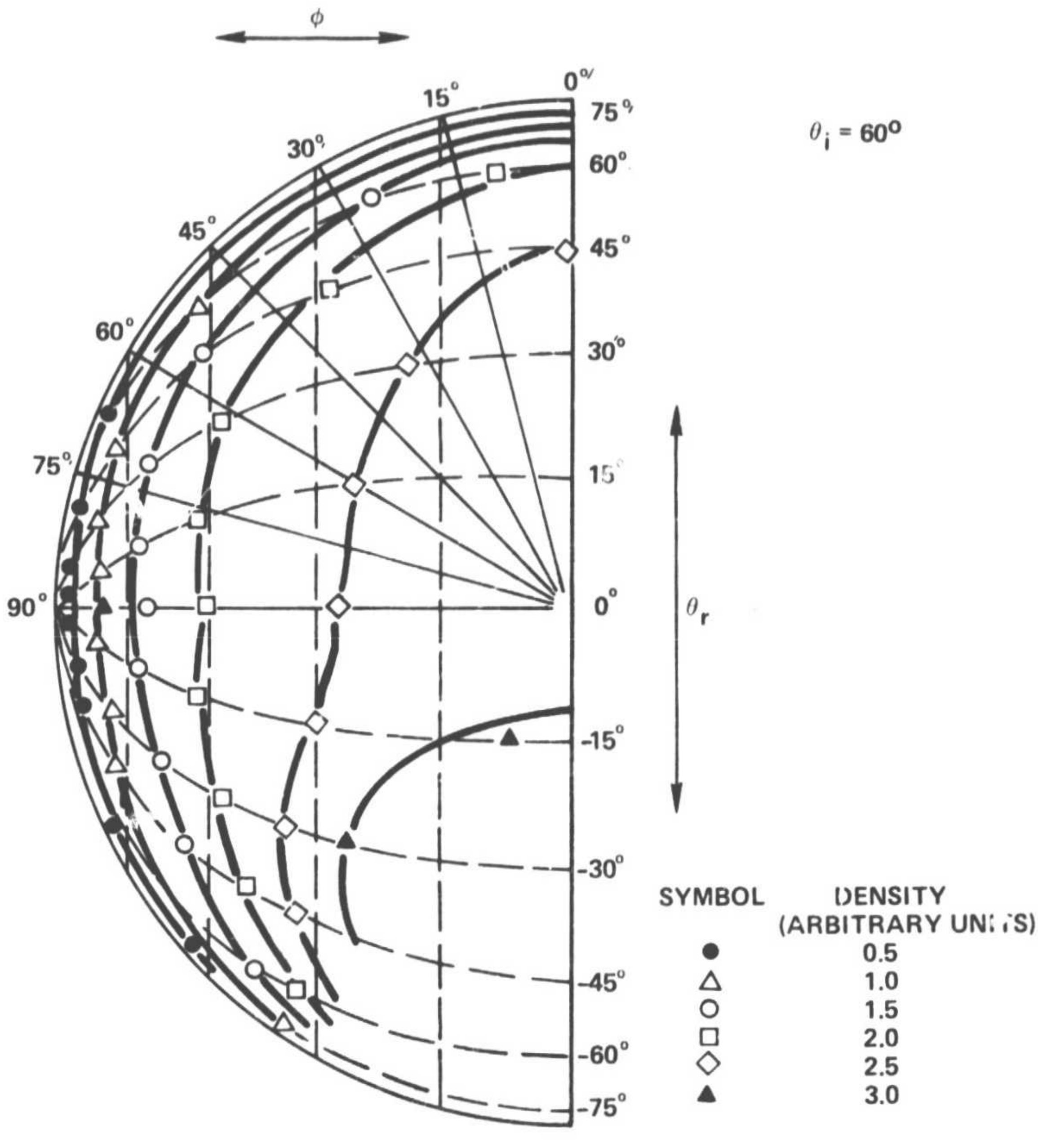

Figure III-5. Polar Plot of Scattered-Beam Density Distribution for 7000 m/sec Helium Beam Scattered from Cleaned 6061-T6 Aluminum Plate at 60° Incidence Angle

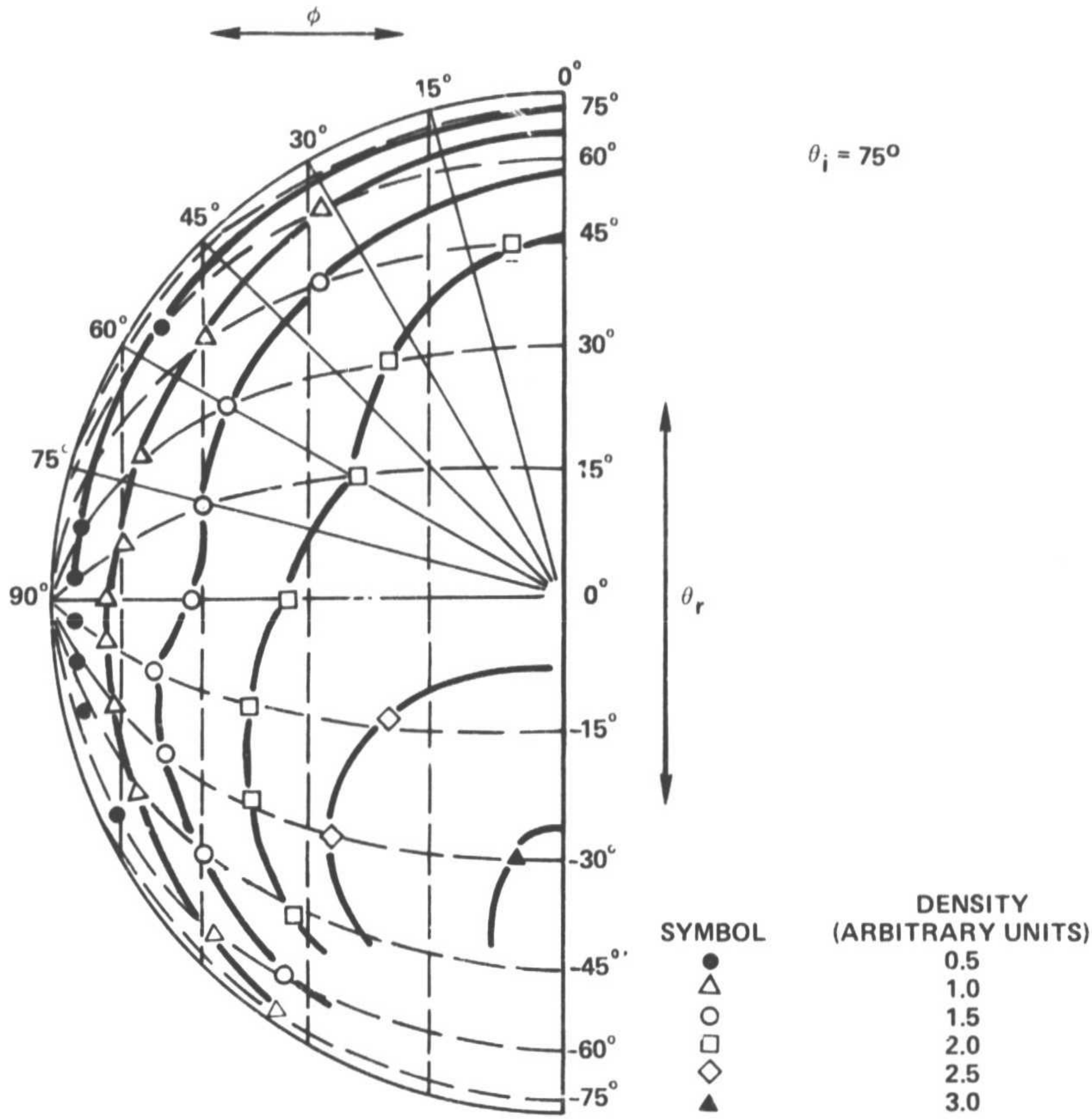

Figure III-6. Polar Plot of Scattered-Beam Density Distribution for 7000 m/sec Helium Beam Scattered from Cleaned 6061-T6 Aluminum Plate at 75° Incidence Angle.

measurements shown here and the energy-distribution measurements to be presented next provide the data required for estimating the overall energy accommodation for this beam-surface combination.

Measurements of energy distributions of satellite-speed helium atoms scattered from a cleaned 6061-T6 aluminum satellite surface were made for six different incidence angles (θ_i = 0°, 15°, 30°, 45°, 60° and 75° from the surface normal). For each incidence angle, distributions were measured at approximately sixty scattering positions. These scattering positions included eleven in-plane scattering angles (θ_r = ±75°, ±60°, ±45°, ±30°, ±15° and 0°) and six out-of-plane scattering angles (ϕ = 0°, 15°, 30°, 45°, 60° and 75°). Typical energy spectra obtained at a given scattering position are shown in Figures III-7 and III-8. Curve A of Figure III-7 represents the energy spectrum of a reflected helium beam superimposed on an energy spectrum of the background helium gas. Curve B of Figure III-7 represents the (thermal) energy of the background helium gas (mostly due to beam load). The reflected beam energy spectrum is then the difference of these two spectra (i.e., A-B). Figure III-8 shows the normalized energy spectra of the thermal background and the reflected helium atoms (Curves 3 and 1), their least-square fitted curves (Curves 4 and 2) and the corresponding differential energy distributions (Curves G and A) obtained using the computer program shown in Appendix A. The differential energy accommodation coefficient was obtained using Equations (II-1) and (II-3). Results for $(A.C.)_E(\theta_i,\theta_r,\phi)$ obtained at all possible scattering angles are given in Tables III-1 to III-6. Measurements were not possible within a solid angle around the incident beam (due to interference between the detector and the incident beam at these scattering positions) and for some glancing scattering angles (due to weak signal-to-noise ratios). These tables also include

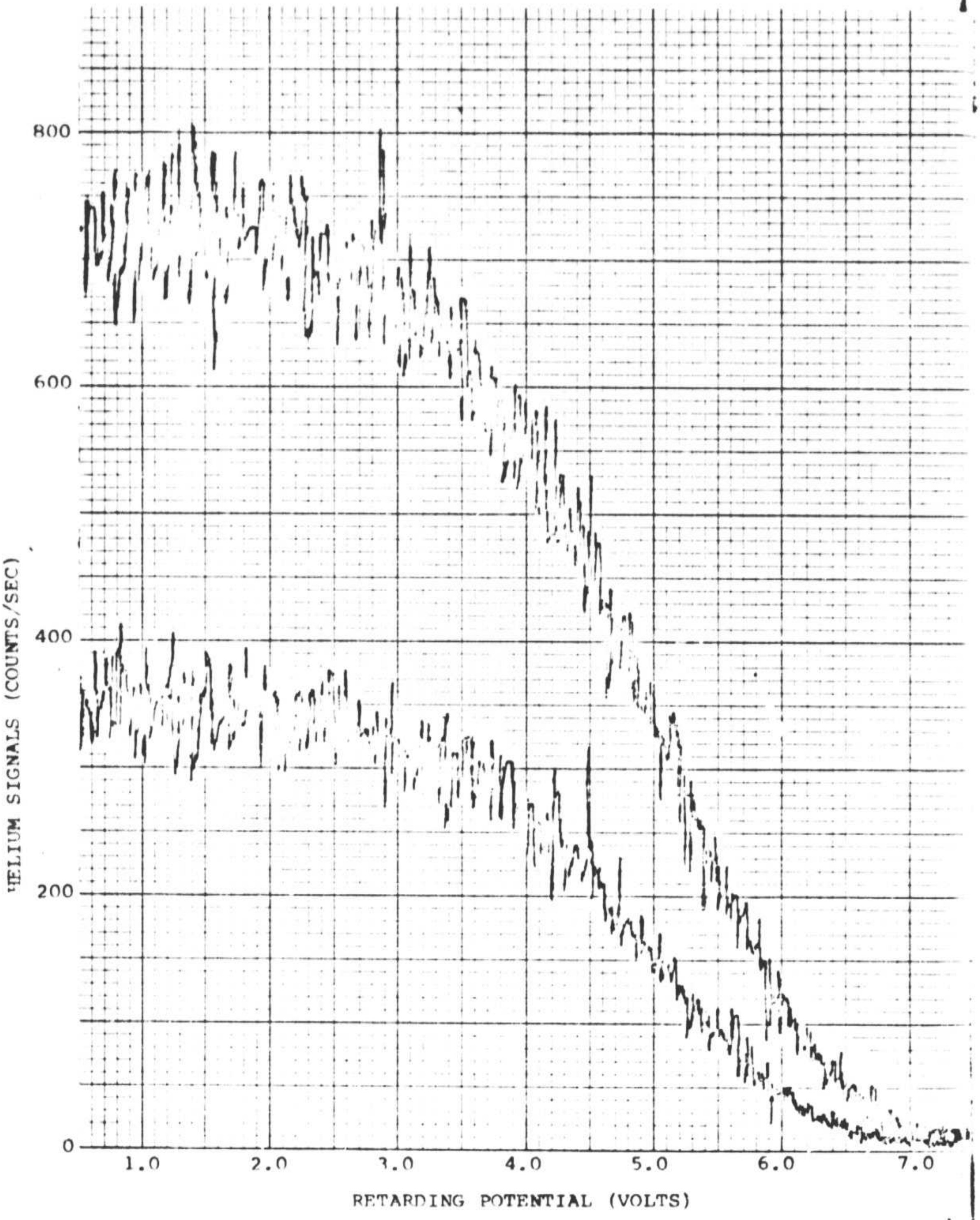

FIGURE III-7 ENERGY SPECTRA OF THE REFLECTED HELIUM ATOMS SUPERIMPOSED ON THE BACKGROUND (CURVE A) AND THE THERMAL BACKGROUND HELIUM GAS (CURVE B)

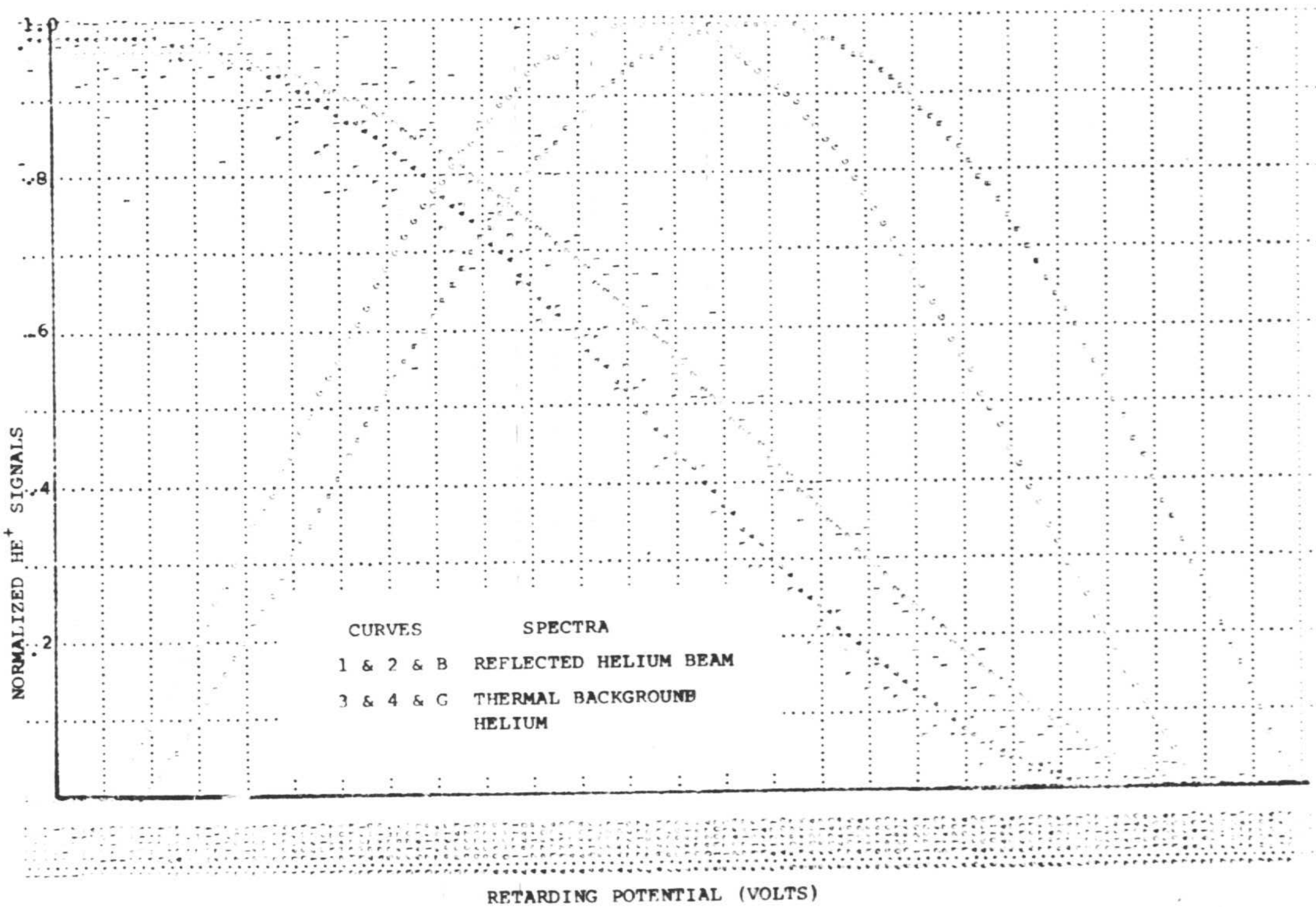

FIGURE III-8 LEAST-SOUARE FITTED ENERGY SPECTRA OF THE REFLECTED HELIUM ATOMS AND THE THERMAL BACKGROUND HELIUM GAS

Table III-1. The Differential Energy Accommodation Coefficients and the Normalized Spatial Density Distribution for 7000 m/sec Helium Beam Scattered From Cleaned 6061-T6 Aluminum Plate at 0^{o} Incidence Angle

ϕ \ θ_r	-75^{o}	-60^{o}	-45^{o}	-30^{o}	-15^{o}	$\pm 0^{o}$	15^{o}	30^{o}	45^{o}	60^{o}	75^{o}
0^{o}	–	43[a] 3.3[b] 16[e]	56 6.6 12						56 6.6 12	43 3.3 16	–
15^{o}	–	55 3.1 14	52 5.9 11						52 5.9 11	55 3.1 14	–
30^{o}	–	63 2.4 15	54 4.4 13						54 4.4 13	63 2.4 15	–
45^{o}	–	–	55 3.3 21	58 4.6 14	55 5.9 11	54 6.4 11	55 5.9 11	58 4.6 14	55 3.3 21	–	–
60^{o}	–	–	–	43 2.4 14	45 3.1 17	46 3.3 17	45 3.1 17	43 2.4 14	–	–	–
75^{o}	–	–	–	–	–	–	–	–	–	–	–

NOTE:

(a) The Differential Accommodation Coefficient (%)
(b) The Normalized Spatial Density (%)
(c) Standard Deviaiton (%)

Table III-2. The Differential Energy Accommodation Coefficients and the Normalized Spatial Density Distribution for 7000 m/sec Helium Beam Scattered from Cleaned 6061-T6 Aluminum Plate at 15° Incidence Angle

ϕ \ θ_r	-75°	-60°	-45°	-30°	-15°	±0°	15°	30°	45°	60°	75°
0°	–	79(a) 3.4(b) 18(c)						48 7.1 14	46 4.8 12	38 3.0 20	–
15°	–	70 3.3 18						48 5.9 18	30 4.3 17	35 2.2 22	–
30°	–	77 2.8 18						47 5.0 18	45 3.4 20	–	–
45°	–	80 2.3 20	76 3.4 11	57 6.1 13	55 6.8 14	52 6.3 12	43 4.8 12	42 3.4 17	–	–	–
60°	–	77 1.6 25	83 2.3 16	61 4.6 20	62 4.8 19	60 4.6 13	55 3.9 19	–	–	–	–
75°	–	–	–	–	–	–	–	–	–	–	–

NOTE:

(a) The differential Accommodation Coefficient (%)
(b) The Normalized Spatial Density (%)
(c) Standard Deviation (%)

Table III-3. The Differential Energy Accommodation Coefficients and the Normalized Spatial Density Distribution for 7000 m/sec Helium Beam Scattered from Cleaned 6061-T6 Aluminum Plate at 30° Incidence Angle.

ϕ \ θ_r	-75°	-60°	-45°	-30°	-15°	±0°	15°	30°	45°	60°	75°
0°	58[a] 1.6[b] 27[c]						51 8.2 11	42 7.2 12	34 4.0 12	45 2.4 21	–
15°	41 1.6 26						48 7.6 11	38 6.2 13	40 3.8 18	50 2.2 21	–
30°	–						47 6.0 12	40 5.0 15	37 3.4 18	–	–
45°	–	67 2.2 19	60 3.0 13	59 4.8 9	57 5.2 11	60 5.0 19	49 4.0 21	40 3.4 20	–	–	–
60°	–	–	64 2.2 18	55 2.6 14	63 3.0 13	49 2.8 17	50 2.4 20	–	–	–	–
75°	–	–	–	–	–	–	–	–	–	–	–

NOTE:

(a) The Differential Accommodation Coefficient (%)
(b) The Normalized Spatial Density (%)
(c) Standard Deviation (%)

Table III-4. The Differential Energy Accommodation Coefficients and the Normalized Spatial Density Distribution for 7000 m/sec Helium Beam Scat*ered from Cleaned 6061-T6 Aluminum Plate at 45° Incidence Angle

θ_r / ϕ	-75°	-60°	-45°	-30°	15°	±0°	15°	30°	45°	60°	75°
0°						49 6.7 10	-55 5.9 10	51 5.2 13	47 3.7 14	19 2.2 19	–
15°						42 6.3 11	41 5.8 10	37 4.9 21	34 3.5 14	25 1.9 20	–
30°						39 5.2 10	38 4.8 10	25 4.1 18	36 3.2 16	–	–
45°	55[a] 1.5[b] 28[c]	74 2.8 19	69 3.9 18	60 4.1 14	59 3.7 13	37 3.7 21	34 3.5 15	23 3.2 20	–	–	–
60°	–	67 1.5 28	56 2.0 28	60 2.2 18	58 2.2 13	21 2.2 30	–	–	–	–	–
75°	–	–	–	–	–	–	–	–	–	–	–

NOTE:

(a) The Differential Accommodation Coefficient (%)
(b) The Normalized Spatial Density (%)
(c) Standard Deviaition (%)

Table III-5. The Differential Energy Accomodation Coefficients and the Normalized Spatial Density Distribution for 7000 m/sec Helium Beam Scattered from Cleaned 6061-T6 Aluminum Plate at 60° Incidence Angle.

ϕ \ θ_r	-75°	-60°	-45°	-30°	-15°	±0°	15°	30°	45°	60°	75°
0°					62 6.2 12	58 5.8 13	63 5.5 15	66 5.2 15	51 5.0 18	–	–
15°					68 6.0 15	71 5.6 20	75 5.2 17	53 5.0 21	52 4.5 11	–	–
30°					70 5.0 17	74 4.9 36	73 4.8 32	56 4.5 11	–	–	–
45°	69[a] 2.0[b] 25[c]	65 2.6 22	61 3.4 19	67 3.8 14	66 4.0 20	74 4.0 36	–	–	–	–	–
60°	–	60 1.6 24	72 2.4 22	70 2.6 23	–	–	–	–	–	–	–
75°	–	–	–	–	–	–	–	–	–	–	–

NOTE:

(a) The Differential Accommodation Coefficient (%)
(b) The Normalized Spatial Density (%)
(c) Standard Deviation (%)

Table III-6. The Differential Energy Accommodation Coefficients and the Normalized Spatial Density Distribution for 7000 m/sec Helium Beam Scattered from Cleaned 6061-T6 Aluminum Plate at 75° Incidence Angle.

ϕ \ θ_r	-75°	-60°	-45°	-30°	-15°	±0°	15°	30°	45°	60°	75°
0°				72 7.0 11	66 6.1 8	64 5.4 13	51 5.0 20	50 4.8 16	45 4.5 30	–	–
15°				63 6.1 11	70 5.8 13	63 5.2 13	59 4.9 20	59 4.5 21	–	–	–
30°				80 5.4 13	60 5.0 13	53 4.5 14	–	–	–	–	–
45°	79[a] 1.9[b] 17	79 2.2 20	84 3.4 18	78 3.9 16	58 4.0 15	–	–	–	–	–	–
60°	66[c] 1.1 23	78 1.8 20	73 2.2 16	75 2.5 16	52 2.5 17	–	–	–	–	–	–
75°	–	–	–	–	–	–	–	–	–	–	–

NOTE:

(a) The Differential Accommodation Coefficient (%)
(b) The Normalized Spatial Density (%)
(c) Standard Deviation (%)

standard deviations (σ) of the reflected-beam energy-spectrum data from the least-square fitted curves and the normalized spatial-distribution function of the reflected helium atoms obtained from the measured spatial distributions shown in Figures III-1 to III-6. The overall energy accommodation coefficients at a given incidence angle was then evaluated using Equations (II-4) and the data given in these tables. The results are shown in Figure III-9.

The differential accommodations obtained show some fluctuations, due perhaps to the weak signal-to-noise ratio which results from the relatively diffusive scattering from the satellite-type aluminum surface. The results also indicate a weak dependence of accommodation on scattering angle, i.e., the $(A.C.)_E(\theta_i,\theta_r,\phi)$ decreases as the scattering direction shifts toward the surface tangent.

The overall accommodation coefficient is slightly higher for a glancing incident beam than for a normal incident beam. The value varies between 50% and 65% for this beam-surface combination.

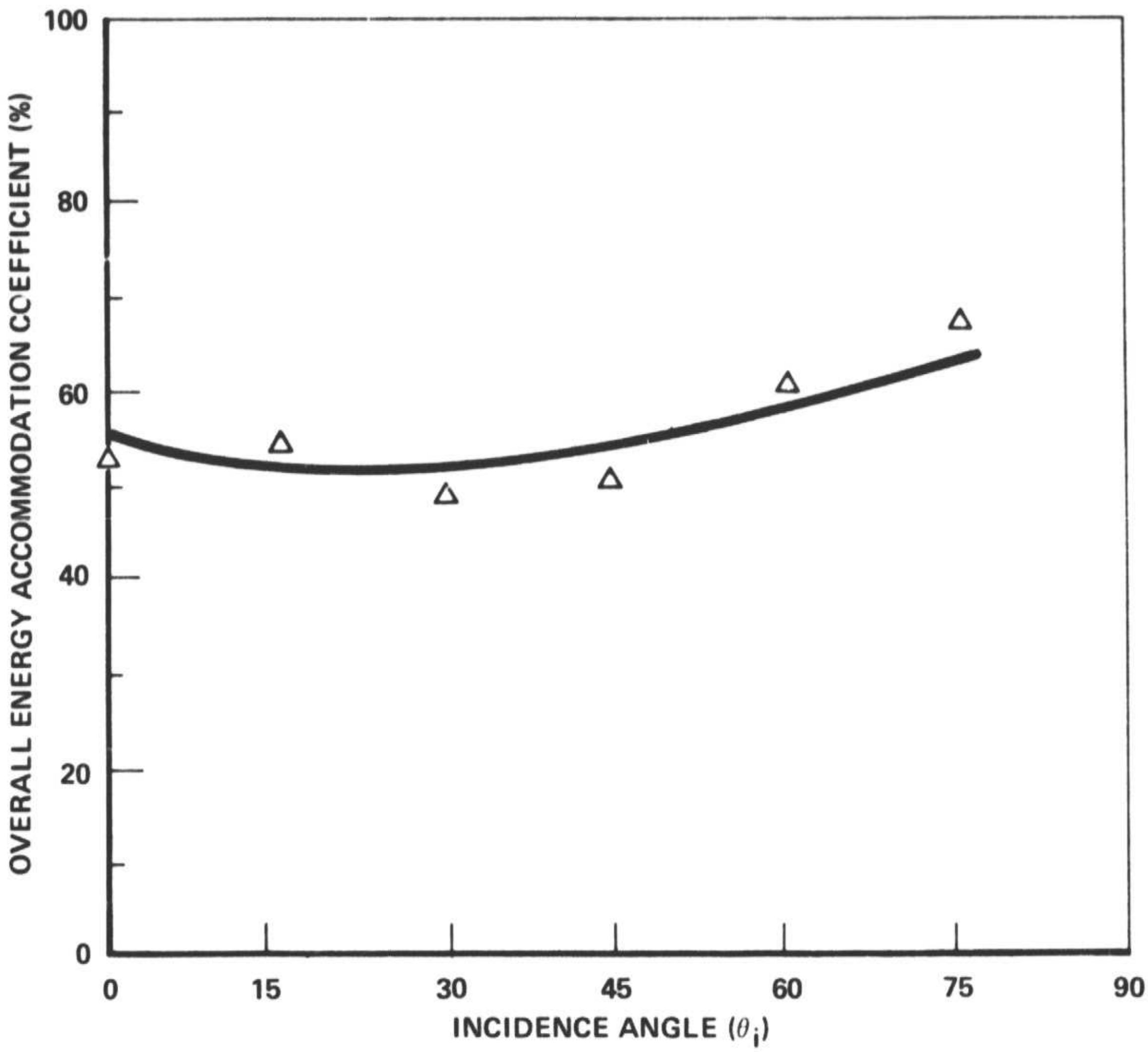

Figure III-9. Overall Energy Accommodation Coefficient of a Satellite-Speed Helium Beam (1.02 eV) Scattered From a Cleaned 6061-T6 Aluminum Surface as a Function of the Incidence Angle.

REFERENCES

1. Liu, S. M., W. E. Rodgers and E. L. Knuth, "Interactions of Satellite-Speed Helium Atoms with Satellite-Surfaces. I: Spatial Distributions of Reflected Helium Atoms," SEAS, UCLA, Report No. UCLA-ENG-7546, 1975.

2. Liu, S. M., "An Experimental Study of Interactions of Hyperthermal Atomic Beams with (111) Silver Surfaces and Adsorbed Molecules," SEAS, UCLA, Report No. UCLA-ENG-7510, 1975.

3. Young, W. S., "An Arc-Heated Ar-He Binary Supersonic Molecular Beam with Energies up to 21 eV," SEAS, UCLA, Report No. 69-39, 1969.

4. Smith, M. C., "Computer Study of Gas Molecule Reflections from Rough Surfaces," Rarefied Gas Dynamics (L. Trilling and H. Wachman, eds.), 2:1217-1220. New York: Academic Press, 1969.

APPENDIX

COMPUTER PROGRAM FOR LEAST-SQUARE FITTING

A. PROGRAM :

```
C
C       MAIN PROGRAM: INPUT; CALL; OUTPUT
C
        DIMENSION NC(512),
       1              Y(512),YBM(512),YBG(512),
       1              DYLS(512),
       1              EM2(2),SIGMA2(2),
       1              GF(251,101),GV(251)
        COMMON /AAA/X(512),YN(512),YLS(512),DY(512),N,EM,SIGMA,KM
        DATA BLANK/1H /,DOT/1H./
        DATA BM/1H1/,BML/1H2/,DBM/1HB/
        DATA BG/1H3/,BGL/1H4/,DBG/1HG/
      1 CONTINUE
        READ (5,800) NSET,KMON,KDAY,KYEAR,THETAI,THETAR,PHI
        IF (NSET.LT.1) GO TO 1000
        WRITE (6,900) KMON,KDAY,KYEAR,THETAI,THETAR,PHI
        IF (NSET.EQ.2) GO TO 5
        IF (NSET.GT.2) NSET=2
        READ (5,810) EI,M,NCV1,V1,NCV2,V2,NI,XLL,NF,XHL,
       1             INTI,INTF,KPG,KSTEP,NPW,NSTEP
        N=NF-NI+1
        DV=(V2-V1)/(NCV2-NCV1+1)
        VI=V1+DV*(NI-NCV1)
        VF=V1+DV*(NF-NCV1)
      5 CONTINUE
        IF (KPG.LT.1) GO TO 35
        DO 10 I=1,251
        GV(I)=0
        DO 10 J=1,101
        GF(I,J)=BLANK
     10 CONTINUE
        DO 20 I=1,251,5
        DO 20 J=1,101
        GF(I,J)=DOT
     20 CONTINUE
        DO 30 I=1,251
        DO 30 J=1,101,10
        GF(I,J)=DOT
     30 CONTINUE
     35 CONTINUE
        DO 40 I=1,32
        K=16*(I-1)
     40 READ (5,830) (YBG(K+J),J=1,16)
        IF (NSET.LT.2) GO TO 55
        DO 50 I=1,32
        K=16*(I-1)
        READ (5,830) (YBM(K+J),J=1,16)
        DO 50 J=1,16
     50 YBM(K+J)=YBM(K+J)-YBG(K+J)
     55 CONTINUE
        DO 500 KI=1,NSET
        DO 60 I=NI,NF
        K=I-NI+1
        NC(K)=I
```

```
      X(K)=VI+DV*(K-1)
      GO TO (61,62),KI
   61 Y(K)=YBG(I)
      GO TO 60
   62 Y(K)=YBM(I)
   60 CONTINUE
      SYMAX=0.0
      SYMIN=0.0
      DO 70 I=1,50
      SYMIN=SYMIN+Y(N-I)
   70 SYMAX=SYMAX+Y(I)
      YMIN=SYMIN/50.0
      YMAX=SYMAX/50.0
      DO 80 K=1,N
      YN(K)=(Y(K)-YMIN)/(YMAX-YMIN)
      IF (YN(K).GE.0.0) GO TC 75
      YN(K)=0.0
   75 IF (YN(K).LE.1.0) GO TO 80
      YN(K)=1.0
   80 CONTINUE
C
C     CALL LEAST-SQUARE CURVE FITTING
C
      CALL LSFCHV(M,XLL,XHL)
      GO TO (110,120),KI
  110 WRITE (6,910)
      GO TO 130
  120 WRITE (6,915)
  130 CONTINUE
      IF (NPW.LT,1) GO TO 200
      WRITE (6,920)
      DO 190 K=1,N,NSTEP
      WRITE (6,930) NC(K),X(K),Y(K),YN(K),YLS(K),DY(K)
  190 CONTINUE
  200 CONTINUE
      EM=0.0
      SIGMA=0.0
      CALL EMEAN(INTI,INTF)
      EM2(KI)=EM
      CALL DEVIA
      SIGMA2(KI)=SIGMA
      SIGMAP=SIGMA*100.0
      WRITE (6,970) EM,SIGMAP
      IF (KPG.LT.1) GO TO 400
      KIN=1
      DO 290 K=1,N,KSTEP
      KIN=KIN+1
      GV(KIN)=X(K)
      JYN=100*ABS(YN(K))+1
      IF (JYN.LT.101) GO TC 291
      JYN=101
  291 CONTINUE
      IF (YLS(K).GE.0.0) GC TO 294
      JYLS=1
      GO TO 292
  294 CONTINUE
      JYLS=100*(ABS(YLS(K)))+1
      IF (JYLS.LT.101) GO TO 292
      JYLS=101
  292 CONTINUE
      JDY=100*ABS(DY(K))+1
      IF (JDY.LT.101) GO TC 293
      JDY=101
  293 CONTINUE
      GO TO (300,310),KI
  300 GF(KIN,JYN)=BG
      GF(KIN,JYLS)=BGL
      GF(KIN,JDY)=DBG
```

```
      GO TO 295
  310 GF(KIN,JYN)=BM
      GF(KIN,JYLS)=BML
      GF(KIN,JCY)=CBM
  295 CONTINUE
  290 CONTINUE
      IF (NSET.GT.1.AND.KI.LT.2) GO TO 400
      WRITE (6,940)
      GV(1)=GV(2)-(GV(3)-GV(2))
      DO 360 I=1,KIN
      WRITE (6,950) GV(I),(GF(I,J),J=1,101)
  360 CONTINUE
  400 CONTINUE
  500 CONTINUE
C
C     CALCULATE TRUE MEAN-BEAM ENERGY
C
      ACC=0.0
      IF (NSET,LT.2) GO TO 600
      ETRUE=EM2(2)-EM2(1)+0.05
      ACC=(EI-ETRUE)/EI*100
  600 CONTINUE
      WRITE (6,975)
      WRITE (6,980) ETRUE,ACC
      WRITE (6,975)
      GO TO 1
  800 FORMAT (4I10,3F10.3)
  810 FORMAT (F5.2,I5,4(I3,F7.2),6I5)
  830 FORMAT (16F5.0)
  910 FORMAT (12X,23H** SET 1: BACKGROUND **/)
  900 FORMAT (///2X,7HDATE : ,I2,1H/,I2,1H/,I2,5X,
     1       26HANGLES(THETAI/THETAR/PHI):,F6.2,1H/,F6.2,1H/,F6.2/)
  915 FORMAT (12X,17H** SET 2: BEAM **/)
  920 FORMAT (3X,7HCH. NO.,12X,3HV-R,11X,5HI-SIG,13X,5HI-NOR,
     1        10X,7HLSI-NOR,8X,9HD(LSI)/DV)
  930 FORMAT (5X,I5,10X,F6.3,10X,F6.1,3(10X,F7.4))
  940 FORMAT (//8X,3HV/R,10X,7H1:I(BM),3X,9H2:LSI(BM),3X,
     1        16HB:D(LSI)/DV-(BM),3X,7H3:I(BG),3X,9H4:LSI(BG),
     2        3X,16HC(LSI)/DV-(BG)//)
  950 FORMAT (2X,F10.5,3X,101A1)
  970 FORMAT (/5X,12HMEAN-ENERGY:,F7.4,3H EV,10X,19HSTANDARD DEVIATION:,
     1        2X,F5.2,1H%/)
  975 FORMAT(//10X,80H**************************************************
     1******************************//)
  980 FORMAT(/10X,22HTRUE MEAN-BEAM ENERGY:,2X,F7.4,3X,2HEV,10X,
     1        26HACCOMMODATION COEFFICIENT=,F7.4,1H%/)
C
 1000 CONTINUE
      STOP
      END


C
      SUBROUTINE LSFCHV(M,XLL,XHL)
C   M >= 2
      DIMENSION T(10),DT(10)
      COMMON /AAA/X(512),Y(512),YLS(512),DY(512),N,EM,SIGMA,KM
      COMMON /SIM/A(100),R(10)
      M1=M+1
C     INITIALIZATION
      DO 2 I=1,M1
    2 R(I)=0.0
      M2=M1*M1
      DO 4 I=1,M2
    4 A(I)=0.0
      XD=2.0/(X(N)-X(1))
      XO=(X(N)+X(1))/(X(N)-X(1))
C     CALCULATE CHEBYSHEV FUNCTION AT TX
      T(1)=1.0
      DO 30 K=1,N
      TX=XD*X(K)-XO
      T(2)=TX
      DO 10 I=3,M1
   10 T(I)=2.0*TX*T(I-1)-T(I-2)
```

```
      DO 20 I=1,M1
      R(I)=R(I)+T(I)*Y(K)
      DO 20 J=1,M1
      IJ=(I-1)*M1+J
   20 A(IJ)=A(IJ)+T(I)*T(J)
   30 CONTINUE
      EPS=1.0E-60
      IER=0
      CALL SIMC(M1,1,EPS,IER)
C     CALCULATE CHEBYSHEV POLYNOMIAL AT TX USING R(I)
C     CALCULATE DY FORM CHEBYSHEV POLYNOMIAL
      DT(1)=0.0
      DT(2)=1.0
      DO 30 K=1,N
      YLSK=0.0
      DYK=0.0
      TX=XD*X(K)-XO
      T(2)=TX
      DO 35 I=3,M1
   35 T(I)=2.0*TX*T(I-1)-T(I-2)
      DO 40 I=1,M1
   40 YLSK=YLSK+T(I)*R(I)
   50 YLS(K)=YLSK
      DO 60 I=3,M1
   60 DT(I)=2.0*(T(I-1)+TX*DT(I-1))-DT(I-2)
      DO 70 I=2,M1
   70 DYK=DYK+R(I)*DT(I)
      IF (DYK.LE.0.0) GO TO 80
      DYK=0.0000001
   80 DY(K)=DYK
      DYM=0.0
      DO 250 K=1,N
      IF (X(K).LT.XLL.OR.X(K).GT.XHL) GO TO 250
  240 IF (DY(K).GT.0.0) GO TO 250
      IF (DYM.GT.ABS(DY(K))) GO TO 250
      DYM=ABS(DY(K))
      KM=K
  250 CONTINUE
      KRS=0
      K=0
  280 K=K+1
      KR=KM-K+1
      IF (KR.LT.1) GO TO 290
      IF (KRS.GT.1) GO TO 285
      DY(KR)=DY(KR)/DYM
      IF (DY(KR).LT.0.0) GO TO 280
      KRS=2
  285 DY(KR)=-0.000001/DYM
      GO TO 280
  290 K=0
      KFS=0
  292 K=K+1
      KF=KM+K
      IF (KF.GT.N) GO TO 300
      IF (KFS.GT.1) GO TO 294
      DY(KF)=DY(KF)/DYM
      IF (DY(KF).LT.0.0) GO TO 292
      KFS=2
  294 DY(KF)=-0.000001/DYM
      GO TO 292
  300 CONTINUE
      RETURN
      END
```

```
      SUBROUTINE DEVIA
      COMMON /AAA/X(512),YN(512),YLS(512),DY(512),N,EM,SIGMA,KM
      SY=0.0
      SQ=0.0
      DO 100 K=1,N
      SY=SY+YN(K)
      DIFF=YN(K)-YLS(K)
  100 SQ=SQ+(ABS(DIFF))**2.0
      SIGMA=(SQ/N)**(0.5)/(SY/N)
      RETURN
      END


      SUBROUTINE EMEAN(INTI,INTF)
      COMMON /AAA/X(512),YN(512),YLS(512),DY(512),N,EM,SIGMA,KM
      SYDE=0.0
      SYEDE=0.0
      KR=0
  280 CONTINUE
      KR=KR+1
      K=KM-KR+1
      IF (K.LT.2.OR.KR.GT.INTI) GO TO 290
      SYDE=SYDE+0.5*(DY(K)+DY(K-1))*(X(K)-X(K-1))
      SYEDE=SYEDE+0.5*(DY(K)+DY(K-1))*0.5*(X(K)+X(K-1))*(X(K)-X(K-1))
      GO TO 280
  290 CONTINUE
      KF=0
  300 CONTINUE
      KF=KF+1
      K=KM+KF
      IF (K.GT.N.OR.KF.GT.INTF) GO TO 310
      SYDE=SYDE+0.5*(DY(K)+DY(K-1))*(X(K)-X(K-1))
      SYEDE=SYEDE+0.5*(DY(K)+DY(K-1))*0.5*(X(K)+X(K-1))*(X(K)-X(K-1))
      GO TO 300
  310 CONTINUE
      EM=SYEDE/SYDE
      RETURN
      END


C
      SUBROUTINE SIMQ(M,N,EPS,IER)
C     DIMENSION A(MM),R(NM)
      COMMON /SIM/A(100),R(10)
      NM=N*M
      MM=M*M
      IF(M) 23,23,1
    1 IER=0
      PIV=0.
      DO 3 L=1,MM
      TB=ABS(A(L))
      IF (TB-PIV) 3,3,2
    2 PIV=TB
      I=L
    3 CONTINUE
      TOL=EPS*PIV
      LST=1
      DO 17 K=1,M
      IF (PIV) 23,23,4
    4 IF (IER) 7,5,7
    5 IF (PIV-TOL) 6,6,7
    6 IER=K-1
    7 PIVI=1./A(I)
      J=(I-1)/M
      I=I-J*M-K
      J=J+1-K
```

```
      DO 8 L=K,NM,M
      LL=L+I
      TB=PIVI*R(LL)
      R(LL)=R(L)
    8 R(L)=TB
      IF (K-M) 9,18,18
    9 LEND=LST+M-K
      IF(J) 12,12,10
   10 II=J*M
      DO 11 L=LST,LEND
      TB=A(L)
      LL=L+II
      A(L)=A(LL)
   11 A(LL)=TB
   12 DO 13 L=LST,MM,M
      LL=L+I
      TB=PIVI*A(LL)
      A(LL)=A(L)
   13 A(L)=TB
      A(LST)=J
      PIV=0.0
      LST=LST+1
      J=0
      DO 16 II=LST,LEND
      PIVI=-A(II)
      IST=II+M
      J=J+1
      DO 15 L=IST,MM,M
      LL=L-J
      A(L)=A(L)+PIVI*A(LL)
      TB=ABS(A(L))
      IF (TB-PIV) 15,15,14
   14 PIV=TB
      I=L
   15 CONTINUE
      DO 16 L=K,NM,M
      LL=L+J
   16 R(LL)=R(LL)+PIVI*R(L)
   17 LST=LST+M
   18 IF (M-1) 23,22,19
   19 IST=MM+M
      LST=M+1
      DO 21 I=2,M
      II=LST-I
      IST=IST-LST
      L=IST-M
      L=A(L)+.5
      DO 21 J=II,NM,M
      TB=R(J)
      LL=J
      DO 20 K=IST,MM,M
      LL=LL+1
   20 TB=TB-A(K)*R(LL)
      K=J+L
      R(J)=R(K)
   21 R(K)=TB
   22 RETURN
   23 IER=-1
      RETURN
      END
```

B. RUN PARAMETER

DATA CARD

#1 READ (NSET, KMON, KDAY, KYEAR, THETAI, THETAR, PHI)

NSET (I10)

> 2: Run with calibration parameters

(or=1) (Data Card #2)

= 2: Run without re-calibrations

KMON, KDAY, KYEAR (3I10)

MONTH/DAY/YEAR

THETAI, THETAR, PHI (3F10.3)

Angular parameters (θ_i,θ_r,ϕ)

#2 (Req. if NSET > 2 or = 1) READ (EI, M, NCVI, VI, NCV2, V2, NI, XLL, NF, XHL, INTI, INTF, KPG, KSTEP, NPW, NSTEP)

EI (F5.2): Incidemt-beam energy

M(I5): Order of the lest-square fitting program

NCVI (I3)
VI (F7.2)
NCV2 (I3)
V2 (F7.2)
} Calibration of x-coordinate

NI (I3)
XLL (F7.2)
NF (I3)
XHL (F7.2)
} Operational limits

INTI (I5)
INTF (I5)
} Integration Limits

KPG (I5): Graphical Index

> 1 : with graphical output

< 1 : without graphical output

KSTEP (I5): Step-size for graphical output

NPW (I5): Output index

> 1 : with detail output

< 1 : without detail output

NSTEP (I5): Step-size for detail output

#3-#28 DATA SET: For thermal background gas

#29-#54 DATA SET: For reflected beam

ENDCARD: (Blank)